Volume 1 | Number 1 | Jan 2013 | Pages 1–100

JAAS

Journal of Analytical Atomic Spectrometry
www.rsc.org/jaas

Selective Chemical Vaporization of Exogenous Tellurium for Characterizing the

Time-Dependent Biodistribution and Dissolution of Quantum Dots in Living Rats

Cheng-Kuan Su, Ting-Yu Cheng, and Yuh-Chang Sun*

Department of Biomedical Engineering and Environmental Sciences, National Tsing-Hua

University, Hsinchu, 30013, Taiwan.

Abstract

Although quantum dots (QDs) are generally toxic substances due to their heavy metal

contents, direct characterization of their dissolution behaviors in living systems remains

complicated because of the dearth of differentiation methods suitable for analyzing their

released components and residual nanostructures. To investigate the degree of QD

dissolution in living rats, in this study we employed a chemical vapor generation scheme

as a novel strategy to selectively vaporize the chalcogen (Te) species released from

CdSeTe/ZnS core/shell QDs (QD705) in rat organ/tissue samples. Under optimized

conditions, we established a chemical differentiation method that exhibited superior

performance and applicability relative to the commonly used filtration method. For rats

intravenously administered with QD705, we used Solvable^{TM} tissue solubilizer to

dissolve the harvested rat tissues. Our experimental results revealed differences in the Te-

and Cd-based biodistribution patterns of QD705; in addition, we found that the ratio of

the concentrations of released Te species from QD705 dissolution to total Te species

(Te_r/Te_{total}) increased in rat blood, liver, and spleen, but decreased in kidney from 2 to 16

weeks post-administration. Therefore, the QD705 administered in living rats must have

dissolved and redistributed progressively during the time course of the experiment,

suggesting that the long-term chemical fate of nanosized materials *in vivo* should be considered in future nanotoxicological research.

Keywords: biodistribution, chemical vaporization, inductively coupled plasma mass spectrometry, quantum dots

* To whom correspondence should be addressed.

Fax: +886-3-5723883, Tel.: +886-3-5727309

e-mail: ycsun@mx.nthu.edu.tw

1. Introduction

Quantum dots (QDs), with their outstanding optical characteristics (including high quantum yields, narrow and tunable emission spectra, and good photostability), are particularly attractive nanomaterials (NMs) with potential biomedical applications.[1-7] Recent progress in surface functionalization of QDs is not only making them the most effective fluorophores for sensing and *in vivo* imaging but also allowing them to enter living animals.[2,5] Nevertheless, once QDs and related NMs are administrated into living animals or discharged into our environment, concerns arising from the adverse biological effects of these substances, and their long-term chemical fate in particular, should be addressed thoroughly.[8-13]

The toxicity of QDs is attributed mainly to their chemical composition [e.g., content of cadmium (Cd), selenium (Se), or tellurium (Te)] and the interactions between biological components and the species released from QDs as they break down or decompose, thereby inducing cytotoxicity similar to that of their individual ions.[9,11,13-16] To assess the toxic effects of QDs in complex systems *in vivo*, a prerequisite is understanding their biodistribution with respect to different exposure routes and their bioaccumulation in preferred and non-preferred organs at each point of time post-administration.[8,9,12,15,17,18] Moreover, the biotransformation of QDs should be monitored carefully because they can be retained within animal bodies for very long periods of time.[11,12,17-21]

Regardless of whether the quantification strategy involves whole-body animal imaging or an absolute quantification strategy after harvesting animal tissue/organ samples, the challenge remains to distinctly determine the contents of the QD nanostructures and their

dissolved ions in living animals.[17-20] Many NMs that do not appear to release their constituent ions in simple aqueous media might release them in biological fluids because of variations in pH conditions or the presence of endogenous chelators that could extract less-coordinated ions from their solid structures.[21] Therefore, interpretations of the adverse effects and toxicological properties of QDs *in vivo* remain limited and problematic.

When evaluating the degrees of QD dissolution and the concentrations of their released species in simple aqueous media, centrifugation and membrane filtration methods are typically selected because of their well-recognized capability for size-discrimination.[22-26] The fractions of released species determined using these approaches can, however, be inconsistent and difficult to compare systematically. The removal of the species released from QDs that strongly or loosely attach to various kinds of proteins or other biomolecules during the size discrimination procedure would lead to inaccurate measurements of the fractions of dissolved species.[27,28] Hence, we are interested in developing more-efficient and more-reliable techniques for rapidly differentiating released species and administered QDs/NMs coexisting in real complicated biological matrices to accurately investigate their biodistribution and, more exactly, to reveal their chemical fates as well as their related toxicities in biological systems.

To differentiate released species and residual QD nanostructures in whole organ/tissue samples, our rationale in this study was based on the dissimilar effects of chemical vapor generation (VG) on dissolved and undissolved chalcogen (Te and Se) species from administered QDs (QD705; CdSeTe/ZnS core/shell nanostructures). The chalcogen species released from QD705 can be converted into the volatile hydrogen telluride (H_2Te)

4

and hydrogen selenium (H_2Se) upon interactions with a strong reducing agent (e.g., $NaBH_4$). In contrast, the native chalcogen species in QD705 would not be vaporized through this conventional chemical VG method because their oxidation state is already at the lowest possible value (-2). Furthermore, because the basal concentration of Te in an animal body is usually too low to be detected,[29,30] the content of Te is a reasonably good indicator of exogenously administrated Te-containing QD705. Although Se is also one of the QD705 constituent elements, the endogenous Se components in rat organs and tissues would hinder the applicability of chemical VG method because it was incapable of distinguishing between endogenous and exogenous sources of Se ions. To measure of the content of Te species and, thereby, infer the degree of QD dissolution *in vivo*, in this study we developed an analytical method based on flow-injection-analysis hydride generation (HG)/inductively coupled plasma mass spectrometry (ICP-MS) to rapidly determine the biodistribution of QDs and the ratios of the concentrations of released Te species from QD dissolution to those of the total Te species in complicated biological samples. To study the degrees of QD705 dissolution in rat blood, liver, spleen, kidney, lung, and brain after an intravenous dosage of 200 pmole QD705 kg^{-1} body weight, we applied the Solvable^TM tissue solubilizer to dissolve the harvested rat tissues while maintaining the integrity of the residual QDs. After optimizing this $NaBH_4$-based chemical vaporization scheme, the solubilized animal samples were mixed with normal phosphate-buffered saline (PBS) solution and divided into two parts. To determine the dissolved Te species resulted from QD705 dissolution, one part was used to directly interact with $NaBH_4$. To determine the total content of Te, we treated the other part of

5

sample with a 10 M HCl solution for completely dissolving the residual QD705

nanostructures and then converted TeO_3^{2-} to H_2Te by interaction with $NaBH_4$.

2. Experimental

2.1 Chemicals

The Qtracker® 705 non-targeted QDs (QD705; Q21061MP, Life Technologies™, Carlsbad, CA, USA) were CdSeTe/ZnS core/shell nanostructures featuring amphiphilic methoxy-PEG-5000 surface coatings and a maximum fluorescence emission at a wavelength of 705 nm. Because their PEGylated surfaces minimize nonspecific biological interactions and immune responses, these commercial QDs have been popular for *in vivo* imaging and nanotoxicological studies.[31-33] Each tube of this product contained 200 μL of a 2 μM solution in 50 mM borate buffer (pH 8.3); the chemical composition (lot number: 1003186) analyzed after acid digestion revealed that the concentrations of Cd, Se, and Te species were 1982 ± 30, 492 ± 9, 34 ± 1 mg L^{-1}, respectively. Stock solutions of Te(IV) and Cd(II) (1000 mg L^{-1}) were obtained from Merck (Darmstadt, Germany). $NaBH_4$ (71321, Sigma–Aldrich, MO, USA), HCl (J. T. Baker, NJ, USA), HNO_3 (J. T. Baker, NJ, USA), and PBS (P3813, Sigma–Aldrich, MO, USA) were employed without further purification. Solvable™ tissue solubilizer (6NE9100, PerkinElmer, IL, USA) was purchased ready-to-use.

2.2 Apparatus and Methods

Fig. 1 and S1 (ESI†) illustrated the schematic representation and concept of our proposed HG–ICP-MS differentiation method for the study of QD dissolution. A dual-channel syringe pump (KDS 260, KD Scientific, MA, USA) and plastic 2.5-mL syringes (4606027V, B. Braun, Melsungen, Germany) were used to load samples into 10-μL polytetrafluoroethylene sample loops positioned on two six-port valves (C22Z-3186,

Valco, Lucerne, Switzerland). The two valves were synchronized and programmed by a single laptop via a serial valve interface (SIV-110, Valco) to switch their positions with a 1-min delay time and consecutively load and inject samples (to avoid the signal overlapping from the two valves; sample throughput: 60 h^{-1}); the detailed operation sequence was provided in Table 1. Samples mixed with an equal volume of PBS (pH 7.4) were used to determine the released Te species from QD705 dissolution; mixing with 10 M HCl was necessary to determine total Te concentrations. The samples in the sample loops were transported by a carrier stream of 0.25 M HCl (0.75 mL min^{-1}) and online-mixed with a 0.05% NaBH$_4$ solution (with 0.1% NaOH; 0.75 mL min^{-1}) through a commercial polyether ether ketone mixing tee (ZT1MFPK, Valco). Without passing through a long reaction coil, the mixture was immediately transported to a commercial gas/liquid separator (GLS; B0507959, PerkinElmer) to separate the volatile H$_2$Te from the aqueous medium. The GLS was made from chemically resistant plastic with an exchangeable PTFE membrane in the screw cap to prevent the liquid from being carried into the ICP torch. The volatile H$_2$Te was online-monitored using an Agilent 7500a ICP mass spectrometer system (Agilent Technologies, CA, USA) with time-resolved scanning at m/z 125 (Te).

2.3 Animal Studies and Sample Preparation

Adult male Sprague–Dawley rats (188 ± 16 g; n = 16) were obtained from BioLASCO (Taiwan). These animals, which were specifically pathogen-free, were acclimatized to their environmentally controlled quarters (25 °C; 12-h light/12-h dark cycle); water and food were available *ad libitum*. All animal treatments and experimental protocols were conducted in conformity with the guidelines and approval of the Institutional Animal

Care and Use Committee at National Tsing-Hua University (approval number: 10051). Eight rats were injected, via tail veins, with 40 pmole QD705 (20 µL of a 2-µM solution) prepared in PBS; the others were injected with PBS as the control group. The rats were sacrificed 2 and 16 weeks post-administration; the rat samples collected included blood, liver, spleen, kidney, lung, and brain.

To maintain the physicochemical properties of the released Te species and residual QD705, tissue solubilization was performed using Solvable^{TM} in a relatively minor sample pretreatment procedure. The rat samples (ca. 0.1 g) were completely dissolved by tenfold (w/v) dilution with Solvable^{TM} and maintained at 60 °C for 2 h. Additional 20-fold dilution of the homogenized samples using PBS solution was necessary to eliminate the matrix effect of biomolecules on the chemical VG method. Rat serum collected from the control group was treated using an identical procedure for use as the sample matrix and to construct calibration curves. Rat organ/tissue samples (ca. 0.2 g) digested with concentrated HNO_3 and heated in a microwave oven (Mars, CEM, Matthews, NC, USA) were used to determine the total Te (m/z 125) and Cd (m/z 111) concentrations through a routine ICP-MS analysis method. All the data are reported as the mean ± standard deviation (SD). Statistical comparisons of Te_r/Te_{total} ratios between the two groups (2 and 16 weeks post-administration) were carried out by Student's two-tailed unpaired t-test and considered to be significantly different when $p < 0.05$.

3. Results and Discussion

3.1 Determination of Ionic Te Species in Original QD Solution

The physicochemical properties of the tested QDs, QD705, have been characterized previously using transmission electron microscopy (TEM) and dynamic light scattering (DLS).[31-33] Because our aim was to differentiate released Te ions from residual QD705, we examined the original ionic Te fraction in this commercial product using a conventional centrifugal filtration method [molecular weight cut-off (MWCO): 3 kDa]. This fraction of diffusible Te species was $0.18 \pm 0.03\%$; hence, we considered QD dissolution to have occurred in our experiments when the concentration ratio of released Te species to total Te species was greater than this original ionic Te fraction.

3.2 Establishment of Chemical Differentiation Method

To employ the chemical VG as a novel working mechanism for chemically differentiating released Te species and residual QDs in animal tissue/organ samples, we selected the TeO_3^{2-} ion as the analyte Te species released from QDs because it does form a H_2Te species when reacted with $NaBH_4$.[34] The critical conditions that allowed vaporization of the dissolved Te species (TeO_3^{2-}), but not Te^{2-} species in QDs, required optimization of the concentration of the reductant ($NaBH_4$), the concentration of HCl in the carrier solution, and the content of the coexisting biological matrix.

By adjusting the concentrations of the reductant and of HCl in the carrier solution to allow chemical differentiation of the two Te species, we compared the signal intensities of H_2Te generated from TeO_3^{2-} and QD705, respectively, under various experimental

conditions. Fig. 2 and S2 revealed that although the differentiation scheme operated at the conditions of higher $NaBH_4$ and HCl (in carrier stream) concentrations would provide better signal intensities for both the two Te species, the maximum difference in sensitivity toward the TeO_3^{2-} and QD705 species (both were prepared in normal PBS solution) occurred when applying 0.05% $NaBH_4$ and 0.25 M HCl (here, the intensity ratio for the two Te species was 57.9 ± 5.4). As the HCl concentrations in the carrier stream increased, both the vaporization efficiencies of TeO_3^{2-} and QD705 increased (Fig. S2) because the hydronium ions (H_3O^+) from HCl solutions would (i) prompt the QD705 dissolution during this transportation process from sample loops to GLS, and (ii) improve the vaporization of TeO_3^{2-} and that dissolved from QD705 nanostructures.[35-37] As a result, a high concentration of HCl in the carrier solution was unfavorable because it led to vaporization of released Te species from the QD705-containing samples.

When QDs/NMs are dispersed in a biological system, a protein corona layer forms immediately on their surfaces; accordingly, the characteristics of the QDs/NMs might be totally different from those in their original status.[38-40] By using DLS, we indeed observed that the average hydrodynamic diameter (intensity-averaged size distribution) of the tested QD705 (20 nM) increased from 44 ± 2 to 53 ± 2 nm after dispersion into 1% fresh rat serum, suggesting the attachment of a 9-nm-thick layer of biomolecules. After preparing solutions of TeO_3^{2-} and QD705 in different concentrations of fresh rat serum, we examined the vaporization efficiencies of the two Te species in terms of the effect of the biological matrix on our chemical VG scheme. Surprisingly, when the concentration of rat serum was 0.5%, we observed almost no volatile H_2Te species generated from the QD705 samples (Fig. 3A) and obtained an intensity ratio for the two Te species of greater

than 5000, confirming that the biological matrix for our developed chemical VG scheme played a critical role in the differentiation of the released Te species from QD705 dissolution and the residual QD705 nanostructures. Nevertheless, the rat serum also suppressed the vaporization efficiency of the TeO_3^{2-} ions. To reach a compromise between the sensitivity and degree of differentiation, we employed 0.5% of the biological matrix as the upper limit for our subsequent analytical studies (the matrix in rat organ and tissue samples were totally 200-fold diluted before being subject to HG process). Thus, chemical differentiation of released Te ions from residual QD nanostructures was feasible through careful adjustment of the concentrations of $NaBH_4$ and HCl (in the carrier solution) as well as the content of biological matrix in the tested samples.

Having verified that our HG-based scheme was capable of selectively measuring the content of free TeO_3^{2-} species originating from QD705, we examined its applicability in the direct determination of the total Te concentration in rat organ/tissue samples. As indicated in Fig. 3B, we required the condition of 5 M HCl to completely decompose QD705 species dispersed in 0.5% rat serum samples and convert them into totally dissolved species. Accordingly, we mixed equal volumes of the Solvable[TM]-treated rat organ/tissue samples and 10 M HCl solution prior to determination of the total Te concentration (both the released Te and residual QD705). For the proposed $NaBH_4$-based hydride generation scheme, the hydronium ions from HCl solutions played an important role in not only improving the vaporization of the dissolved Te from QD705 dissolution[35-37] but also prompting the dissolution of the residual QD705 nanostructures for the total Te measurement. As the treated HCl concentrations increased, the vaporization efficiencies of the residual QD705 nanostructures increased because QD705

12

was first dissolved and then vaporized through the facilitation of hydronium ions. Our results also indicated that a 3.75-M HCl solution was capable of efficiently dissolving all the remaining QD705 nanostructures in rat serum samples, allowing the equal sensitivity of the two Te species.

After QD705 administration and dissolution, rat organs and tissues contained both the dissolved Te species and non-dissolved Te species remaining in residual QD705 nanostructures. If these samples were treated with HCl solutions, the additional dissolution of the originally non-dissolved Te species would be promoted by the added hydronium ions and led to bias in Te_r/Te_{total} ratios. Therefore, we adopt normal PBS as a conditioning solution and conduct the experiments in the range of non-maximal signal intensities mainly due to the vaporization of the released Te species without altering the original equilibrium status between the dissolved Te species and residual QD705 nanostructures in rat organ and tissue samples. Based on our experiments described above, mixing the Solvable^{TM}-treated rat organ/tissue sample with 10 mM PBS (pH 7.4) and 10 M HCl solutions, respectively, allowed quantification of the released Te species and total Te species in the same analytical sequence.

The optimization of the operation flow rates of reductant and carrier solution was provided in the Fig. S3. After method optimization and a successful feasibility study, we evaluated the analytical performance under the optimized operating conditions (Table 2). From calibration curves for TeO_3^{2-} and QD705 species (10–500 ng L^{-1}) prepared in 0.5% fresh rat serum (Table 3 and Fig. S4), we determined the limits of detection (three times the SD of the baseline noise; $n = 7$) were 0.4 and 1.8 ng L^{-1}, respectively, for the total Te concentration (sample premixed with 10 M HCl) and the released Te species (sample

13

premixed with PBS solution). Because of the superior transportation efficiency of gaseous species in the HG–ICP-MS analysis mode, the analytical sensitivity of our system was greater than that of routine ICP-MS analysis when determining the total Te concentration. Moreover, we examined the method's accuracy and applicability by testing 0.5% rat serum samples spiked with TeO_3^{2-} and QD705 at various concentrations, providing different concentration ratios of TeO_3^{2-} to total Te. In Fig. 4, the slope of the expected-to-measured ratio of TeO_3^{2-}/Te_{total} was 0.9979 (ideally, this ratio should be 1). In other words, neither the high salt content nor the complicated biological matrix had a significant influence on the method's accuracy when differentiating released Te species from QD705 nanostructures. We have adopted Se as an indicator to state QD705 dissolution in biological system; however, our results indicated that the endogenous Se species in rat organs and tissues made the differentiation of released Se species from residual QD705 nanostructures infeasible since the expected-to-measured ratio of SeO_3^{2-}/Se_{total} was only 0.2747 for 0.5% rat serum samples (Fig. S5, ESI†).

We also applied membrane-based centrifugal filtration (MWCO: 3 kDa) as a general strategy to study the QD705 dissolution behavior.[41-43] It revealed that even though the released Te species from QD705 dissolution were probably anionic, their adhesion to biomolecules was weak relatively to that of cationic species,[44] with a 12–% slope departure (slope = 0.8789) between the expected and measured ratios in the samples containing 0.5% rat serum (Fig. S6, ESI†). When we used this filtration method to separate the cationic species (e.g., Cd^{2+}) co-released from QD705, the slope of the expected-to-measured ratio was only 0.5726, suggesting that the bias between the measured and exact Cd^{2+} fractions was greater than 40%. This comparison also implies

that interpretations of the toxic effects of QDs resulting from their released species, as evaluated using membrane filtration methods, might be erroneous because they mostly ignore the interactions between the freely dissolved ionic species and complicated biological molecules. In contrast, our developed chemical VG-based differentiation scheme is not only simple and sensitive but also reliable when evaluating the degrees of QD dissolution in complicated biological systems.

Maintaining the original physicochemical properties of the released Te species and QD705 after physical/chemical pretreatment is of paramount importance when studying QD dissolution from harvested animal samples. Treatment of tissue samples with alkaline tetramethylammonium hydroxide (TMAH) has been reported to extract NMs and their constituent ions.[45,46] In this study, we adapted a convenient solubilization protocol (samples were completely dissolved by tenfold dilution with Solvable[TM] and then heating at 60 °C for 2 h)[47,48] to dissolve the harvested rat samples as well as maintain the original integrity of the two distinct Te-containing species. Analyses of control rat samples, including blood, liver, spleen, kidney, lung, and brain, spiked with TeO_3^{2-} or QD705 before and after performing the solubilization provided data within the acceptable spike recoveries (84–118%, Table 4), suggesting that (i) the pretreatment of rat samples using this solubilization procedure did not alter the original properties of the released Te species or QD705 and successfully met the requirements for hyphenation to our HG–ICP-MS method, and (ii) adopting rat serum as a sample matrix to calibrate others organ and tissue samples was justified and chemical VG method was tolerant to complicated biological matrix.

3.3 Biodistribution and Dissolution of QD705 in Living Rats

Fig. 5 demonstrated the time-resolved signal intensities of Te for the spleen samples of control rat spiked with TeO_3^{2-} and QD705 (0.1 µg Te L^{-1}) respectively and the rat spleen sample 2 weeks post-administration [200 pmole QD705 kg^{-1} body weight (as 3.4 µg Te kg^{-1} body weight)]. It clearly illustrated that our proposed HG–ICP-MS differentiation scheme only vaporized the TeO_3^{2-} species without the signal contributions from the residual QD705 nanostructures, and QD705 dissolved and released Te species which would potentially redistribute to others rat organs and tissues. We then obtained the element-related biodistribution of QD705 at 2 and 16 weeks post-administration, based on the respective quantification of Te and Cd (Table 5). Interestingly, the profiles of the Cd-based biodistribution patterns of QD705 were similar to that reported by the Lin group;[49,50] there were, however, apparent discrepancies between the Te- and Cd-based biodistribution patterns of the administrated QD705. The total administrated Cd species, including the fraction in residual QD705 and the released fraction, were characteristically deposited in the liver, spleen, and kidney; in contrast, the total Te species tended to accumulate in all of the observed organs and tissues, especially at 16 weeks post-administration. Accordingly, using a single element to evaluate the overall biodistribution of administrated NMs in a living organism might result in misinterpretation of the long-term chemical fate because of dissolution and redistribution of the released species.

In addition, through our developed chemical VG-based differentiation method, we found that the Te_r ($Te_{released}$)/Te_{total} ratios increased from 2 to 16 weeks post-administration in the rat blood, liver, and spleen, but changed insignificantly in the lung and brain and decreased in the kidney. To the best of our knowledge, this study is first to directly identify the time-dependent degradation of QD705 *in vivo* in conjunction with

16

systemic redistribution of the released species. Our experimental results indicate that quantification data from a single component (Cd, Te, or Se) of QD705 do not actually reflect the biodistribution patterns and dynamic changes in the organ/tissue deposition of the nanostructures or of their released components. Accordingly, more extensive analyses should be performed to determine the chemical fates of QDs in biological systems.

According to the available scientific reports about the fate of chalcogen-containing QDs *in vivo*, (i) Wiecinski *et al*. have illustrated the similar dose-response curves for the co-exposure of Cd^{2+} and SeO_3^{2-} compared to the oxidatively weathered CdSe/ZnS QDs,[51] (ii) Mahendra *et al*. have identified that the released Se from the QD655 (Life Technologies[TM]) in the solution condition of pH 7 was 99% SeO_3^{2-},[52] and (iii) Qu *et al*. also found that Se^{2-} in CdSe/ZnS QDs exposed to *Caenorhabditis elegans* was oxidized to SeO_3^{2-} based on comparing the *in situ* Se K edge microbeam X ray absorbance near edge structure spectra of the tested QDs in the worm's pharynx or intestine with the characteristic peak of Na_2SeO_3.[53] Since Te and Se were in the same group of the periodic table and with the equal oxidation states (–2) in QD705 nanostructures, in this study we adopted inorganic TeO_3^{2-} ions as a measure of possibly released Te species. It is possible, however, that the Te species distributed in rats might be other inorganic, methylated, or sugar-containing species. Based on our results, with the exception of the rat blood content 16 weeks post-administration, we observed no significant differences between the total Te concentrations determined using our HG–ICP-MS method and the commonly used routine analysis method (Table S1, ESI†), revealing that the total Te species in the rat samples pretreated with 10 M HCl were availably vaporized for studying the QD705 dissolution, rather than possessing a species-dependent vaporization behavior (TeO_4^{2-}

cannot be vaporized by $NaBH_4$).[34] Besides, we have also used C_{18} cartridge to remove nonpolar organic Te species[54,55] and determine the difference in Te concentrations in solubilized rat organ and tissue samples without and with C_{18} pretreatment. As indicated in Fig. S7, the most Te in rat organs and tissues might be present as inorganic form. Although obtaining a detailed understanding of the Te species released in living rat samples was not the emphasis of this study, our initial assumption of using TeO_3^{2-} as a candidate Te species for identifying QD705 nanostructures and their dissolution in the rat liver, spleen, kidney, lung, and brain was an acceptable one.

Current research into QD toxicity in living biological systems almost always focuses on their abnormal physiological responses and induced toxic effects upon applying different administration routes,[9,11-16] even for QDs featuring highly biocompatible surface passivation. Few studies have directly probed QD dissolution behavior and kinetics. The blue-shifted fluorescence emission spectra of injected (CdSe)ZnS core/shell QDs in mice liver, spleen, and lymph nodes have been observed two years post-administration;[56] the Cd-to-Te ratio in mice kidney has been observed to increase after a 16-week administration of (CdSeTe)ZnS core/shell QDs, suggesting the accumulation of released Cd ions.[50] Although those two studies reveal implicitly that QD nanostructures do change in living animals, quantification of the ions released from those QD nanostructures—the most critical factor for QD nanotoxicity—was determined indirectly.

When Cd-containing QDs undergo dissolution, both Cd ions and chalcogen species (S, Se, and Te) are released simultaneously. Whereas Cd ions are known to inhibit DNA, RNA, and protein synthesis, as well as break down DNA strands and mutate chromosomes,[11,57] the toxic effects of these chalcogens have rarely been investigated.

The species released from the dissolution of QD705 are Cd, Se, Te, and Zn, ions, all of which have been found, after intravenous administration, to perturb signaling pathways in the kidney,[58,59] induce metallothionein production in renal epithelial cells,[50] and disrupt the cellular antioxidant system that leads to hepatotoxicity.[31] In addition to majorly concerning the released Cd ions, our results suggested that after QD705 dissolution, all of the constituent elements are candidates for disclosing their dissolution behaviors and eliciting adverse biological effects *in vivo*. Using the unique species-dependent effects of $NaBH_4$ on the reduction on Te species, our chemical VG-based scheme allows unambiguous differentiation of the Te species released from residual QD705 nanostructures. Because the chemical VG strategy can convert various elements, including silver (Ag), gold (Au), copper (Cu), platinum (Pt), titanium (Ti), arsenic (As), mercury (Hg), and zinc (Zn), into volatile species,[60] we anticipate that, after suitable optimization of experimental conditions for each element and associated NM, our proposed analytical scheme should be capable of differentiating many other kinds of released ionic species from their parent MNs.

4. Conclusions

We have developed a new analytical scheme for the differentiation of released Te species and those in residual QD705 nanostructures based on the species-dependent vaporization behavior of Te species reduced using $NaBH_4$. After optimizing each parameter, we demonstrated that the analytical capability of this chemical differentiation method is superior to that of the conventional filtration-based separation method. We observed an apparent discrepancy in the element-based biodistribution patterns after intravenous administration; the dissolution of QD705 and the redistribution of released species proceeded continuously in rat organs and tissues. Accordingly, our results have important implications for the current nanotoxicological research into QDs; we suggest that more emphasis be placed on investigating the long-term chemical fate of administrated NMs.

Acknowledgment

References

1. U. Resch-Genger, M. Grabolle, S. Cavaliere-Jaricot, R. Nitschke, T. Nann, *Nat. Method*, 2008, **5**, 763–775.

2. I. L. Medintz, H. T. Uyeda, E. R. Goldman, H. Mattoussi, *Nat. Mater.*, 2005, **4**, 435–446.

3. J. M. Klostranec, W. C. W. Chan, *Adv. Mater.*, 2006, **18**, 1953–1964.

4. T. Jamieson, R. Bakhshi, D. Petrova, R. Pocock, M. Imani, A. M. Seifalian, *Biomaterials*, 2007, **28**, 4717–4732.

5. N. Erathodiyil, J. Y. Ying, *Acc. Chem. Res.*, 2011, **44**, 925–935.

6. H. Mattoussi, G. Palui, H. B. Na, *Adv. Drug Deliv. Rev.*, 2012, **64**, 138–166.

7. C. E. Probst, P. Zrazhevskiy, V. Bagalkot, X. Gao, *Adv. Drug Deliv. Rev.*, 2013, **65**, 703–718.

8. A. Nel, T. Xia, L. Maodler, N. Li, *Science*, 2006, **311**, 622–627.

9. H. C. Fischer, W. C. W. Chan, *Curr. Opin. Biotech.*, 2007, **18**, 565–571.

10. H. F. Krug, P. Wick, *Angew. Chem. Int. Ed. Engl.*, 2011, **50**, 1260–1278.

11. M. Bottrill, M. Green, *Chem. Commun.*, 2011, **47**, 7039–7050.

12. K. Yong, W. Law, R. Hu, L. Ye, L. Liu, M. T. Swihart, P. N. Prasad, *Chem. Soc. Rev.*, 2013, **42**, 1236–1250.

13. J. M. Tsay, X. Michalet, *Chem. Biol.*, 2005, **12**, 1159–1161.

14. B. A. Rzigalinski, J. S. Strobl, *Toxicol. Appl. Pharmacol.*, 2009, **238**, 280–288.

15. J. L. Pelley, A. S. Daar, M. A. Saner, *Toxicol. Sci.*, 2009, **112**, 276–296.

16. K. M. Tsoi, Q. Dai, B. A. Alman, W. C. W. Chan, *Acc. Chem. Res.*, 2013, **46**, 662–671.

17. E. Pic, L. Bezdetnaya, F. Guillemin, F. Marchal, *Anti-Cancer Agents Med. Chem.*, 2009, **9**, 295–303.

18. S. Li, L. Huang, *Mol. Pharm.*, 2008, **5**, 496–504.

19. B. Wang, W. Feng, Y. Zhao, Z. Chai, *Metallomics*, 2013, **5**, 793–803.

20. X. He, Y. Ma, M. Li, P. Zhang, Y. Li, Z. Zhang, *Small*, 2013, **9**, 1482–1491.

21. G. V. Lowry, K. B. Gregory, A. C. Apte, J. R. Lead, *Environ. Sci. Technol.*, 2012, **46**, 6893−6899.

22. A. M. Derfus, W. C. W. Chan, S. N. Bhatia, *Nano Lett.*, 2004, **4**, 11–18.

23. M. C. Henson, P. J. Chedrese, *Exp. Biol. Med.*, 2004, **229**, 383–392.

24. M. C. Mancini, B. A. Kairdolf, A. M. Smith, S. Nie, *J. Am. Chem. Soc.*, 2008, **130**, 10836–10837.

25. H. C. Fischer, T. S. Hauck, A. Gómez-Aristizábal, W. C. W. Chan, *Adv. Mater.*, 2010, **22**, 2520–2524.

26. M. Xu, G. Deng, S. Liu, S. Chen, D. Cui, L. Yang, G. Wang, *Metallomics*, 2010, **2**, 469–473.

27. T. Tsai, *J. Chromatogr. B*, 2003, **797**, 161–173.

28. S. V. Deshmukh, A. Harsch, *J. Pharmacol. Toxicol. Methods*, 2011, **63**, 35–39.

29. L. M. Klevay, *Pharmac. Ther. A*, 1976, **1**, 223–229.

30. Y. Ogra, R. Kobayashi, K. Ishiwata, K. T. Suzuki, *J. Inorg. Biochem.*, 2008, **102**, 1507–1513.

31. C. Lin, M. Yang, L. W. Chang, C. Yang, H. Chang, W. Chang, M. Tsai, C. Wang, P. Lin. *Nanotoxicology*, 2011, **5**, 650–663.

32. C. C. Ho, H. Chang, H. T. Tsai, M. H. Tsai, C. S. Yang, Y. C. Ling, P. Lin, *Nanotoxicology*, 2013, **7**, 105–115.

33. C. Ho, Y. Luo, T. Chuang, C. Yang, Y. Ling, P. Lin, *Toxicology*, 2013, **308**, 1–9.

34. E. Yildirim, P. Akay, Y. Arslan, S. Bakirdere, O. Y. Ataman, *Talanta*, 2012, **102**, 59–67.

35. R. Kobayashi, K. Imaizumi, *Anal. Sci.*, 1991, **7**, 447–450.

36. A. D'Ulivo, J. Dědina, Z. Mester, R. E. Sturgeon, Q. Wang, B. Welz, *Pure Appl. Chem.*, 2011, **83**, 1283–1340.

37. P. Pohl, *TRAC–Trends Anal. Chem.*, 2004, **23**, 87–101.

24

38. I. Lynch, T. Cedervall, M. Lundqvist, C. Cabaleiro-Lago, S. Linse, K. A. Dawson, *Adv. Colloid Interface Sci.*, 2007, **134–135**, 167–174.

39. I. Lynch, K. A. Dawson, *Nanotoday*, 2008, **3**, 40–47.

40. I. Lynch, A. Salvati, K. A. Dawson, *Nat. Nanotechnol.*, 2009, **4**, 546–547.

41. A. Galeone, G. Vecchio, M. A. Malvindi, V. Brunetti, R. Cingolani, P. P. Pompa, *Nanoscale*, 2012, **4**, 6401–6407.

42. M. Hadioui, S. Leclerc, K. J. Wilkinson, *Talanta*, 2013, **105**, 15–19.

43. I. Corazzari, A. Gilardino, S. Dalmazzo, B. Fubini, D. Lovisolo, *Toxicol. In Vitro*, 2013, **27**, 752–759.

44. C. Mizuno, S. Bao, T. Hinoue, T. Nomura, *Anal. Sci.*, 2005, **21**, 281–286.

45. Z. Arslan, M. Ates, W. McDuffy, M. S. Agachan, I. O. Farah, W. W. Yu, A. Bednar, *J. Hazard. Mater.*, 2011, **192**, 192–199.

46. B. Schmidt, K. Loeschner, N. Hadrup, A. Mortensen, J. J. Sloth, C. B. Koch, E. H. Larsen, *Anal. Chem.*, 2011, **83**, 2461–2468.

47. B. A. Magnuson, J. Appleton, G. B. Ames, *J. Agric. Food Chem.*, 2007, **55**, 1033–1038.

48. K. Doudrick, N. Corson, G. Oberdorster, A. C. Eder, P. Herckes, R. U. Halden, P. Westerhoff, *ACS Nano*, 2013, **7**, 8849–8856.

49. R. S. H. Yang, L. W. Chang, J. Wu, M. Tsai, H. Wang, Y. Kuo, T. Yeh, C. S. Yang, P. Lin, *Environ. Health Perspect.*, 2007, **115**, 1339–1343.

50. C. Lin, L. W. Chang, H. Chang, M. Yang, C. Yang, W. Lai, W. Chang, P. Lin *Nanotechnology*, 2009, **20**, 215101.

51. P. N. Wiecinski, K. M. Metz, T. C. K. Heiden, K. M. Louis, A. N. Mangham, R. J. Hamers, W. Heideman, R. E. Peterson, J. A. Pedersen, *Environ. Sci. Technol.*, 2013, **47**, 9132–9139.

52. S. Mahendra, H. Zhu, V. L. Colvin, P. Alvarez, *Environ. Sci. Technol.*, 2008, **42**, 9424–9430.

53. Y. Qu, W. Li, Y. Zhou, X. Liu, L. Zhang, L. Wang, Y. Li, A. Iida, Z. Tang, Y. Zhao, Z. Chai, C. Chen, *Nano Lett.*, 2011, **11**, 3174–3183.

54. J. L. Gomez-Ariza, J. A. Pozas, I. Giraldez, E. Morales, *Analyst*, 1999, **124**, 75–78.

55. N. P. Vela, D. T. Heitkemper, K. R. Stewart, *Analyst*, 2001, **126**, 1011–1017.

56. J. A. J. Fitzpatrick, S. K. Andreko, L. A. Ernst, A. S. Waggoner, B. Ballou, M. P. Bruchez, *Nano Lett.*, 2009, **9**, 2736–2741.

57. M. Green, E. Howman, *Chem. Commun.*, 2005, **41**, 121–123.

58. P. Lin, J. Chen, L. W. Chang, J. Wu, L. Redding, H. Chang, T. Yeh, C. S. Yang, M. Tsai, H. Wang, Y. Kuo, R. S. H. Yang, *Environ. Sci. Technol.*, 2008, **42**, 6264–6270.

59. C. Lin, L. W. Chang, Y. Wei, S. Wu, C. Yang, W. Chang, Y. Chen, P. Lin, *Kaohsiung J. Med. Sci.*, 2010, **28**, S53–S62.

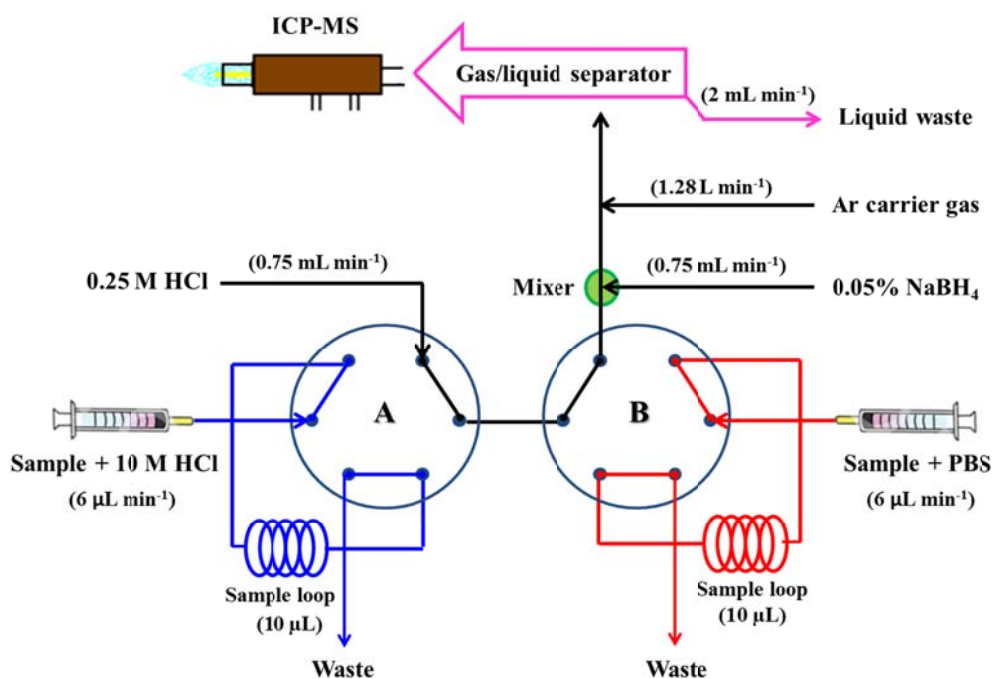60. P. Pohl, *TRAC–Trends Anal. Chem.*, 2004, **23**, 21–27.

Fig. 1. Schematic representation of the established HG-ICP-MS differentiation system. A,

B: Six-port, two-position valve. Valves A and B were programmed by a laptop through

the Valco serial valve interface.

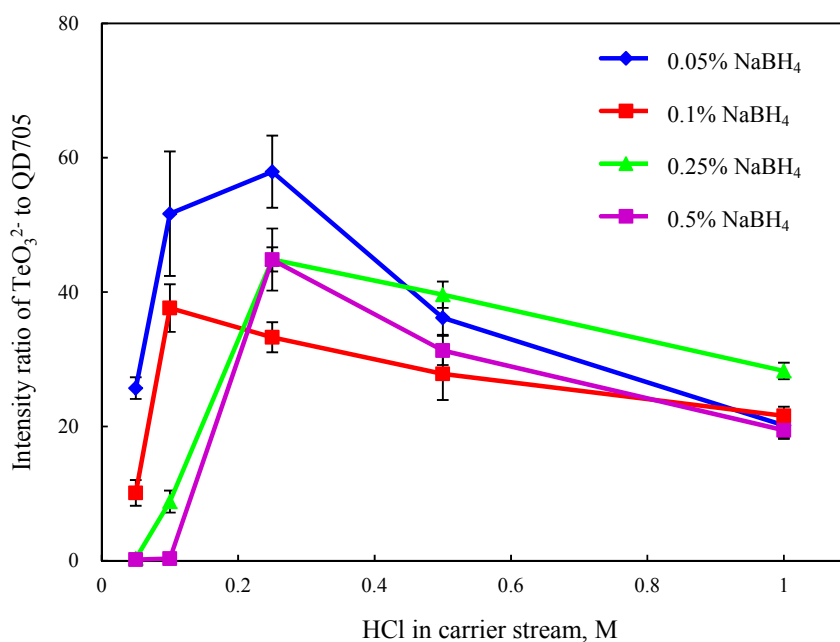**Fig. 2.** Intensity ratios of TeO_3^{2-} to QD705 plotted with respect to the $NaBH_4$ and HCl (carrier solution) concentrations for the established chemical VG scheme. Values are expressed as the ratio of the signal intensity of TeO_3^{2-} to that of QD705 under the condition of an equal concentration (1 μg Te L^{-1}) of the two species. Error bars represent SDs ($n = 5$).
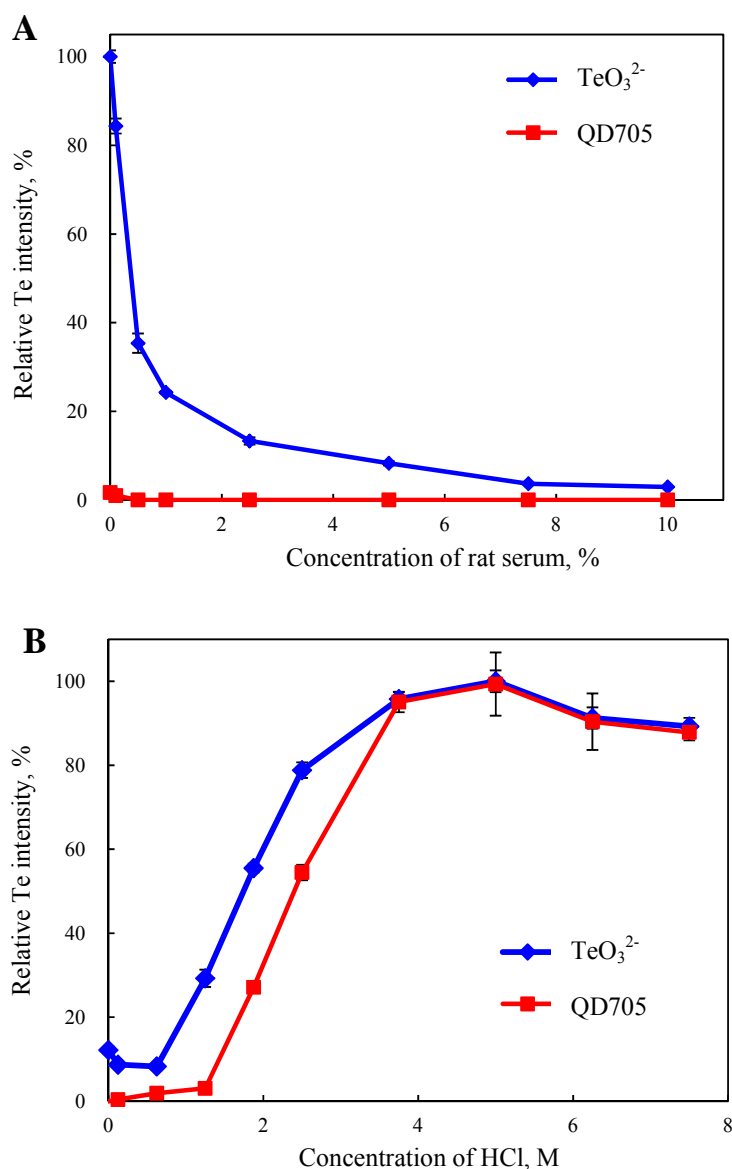
Fig. 3. Relative intensities of TeO_3^{2-} and QD705 plotted with respect to (A) rat serum concentration in samples and (B) HCl treatment (0.5% rat serum sample) for the chemical VG scheme. Concentration of both Te species: 1 µg Te L^{-1}. The signals were all normalized to the values of their respective maximum intensities [QD705 in serum-free PBS for (A), and TeO_3^{2-} at a condition of 5M HCl for (B)]. Error bars represent SDs ($n =$ 5).
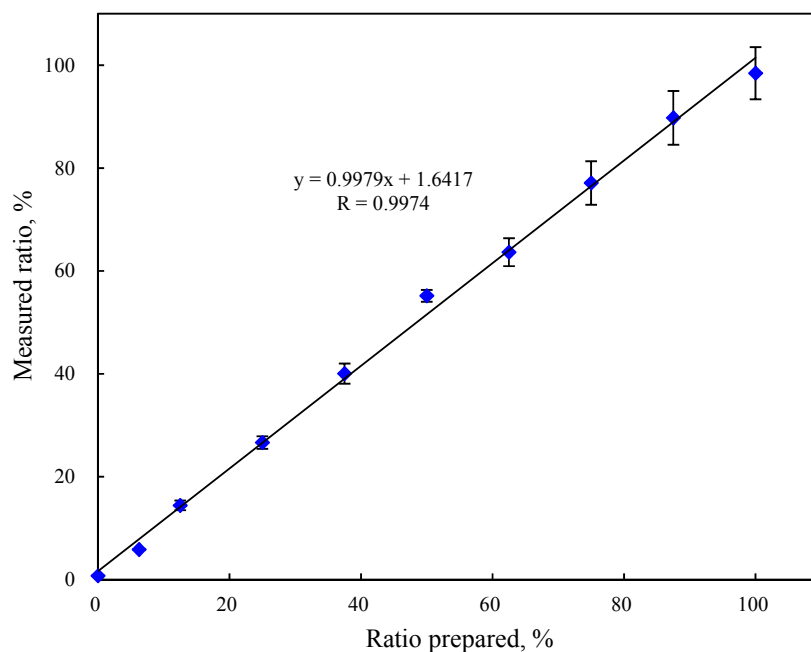
Fig. 4. Correlations between expected and experimentally measured TeO_3^{2-}/Te_{total} ratios determined using our developed HG–ICP-MS system. The totally spiked Te concentrations of the two species were fixed at 0.5 μg L^{-1}. Error bars represent SDs (n = 5).

Fig. 5. Signal profile of Te (*m/z* 125) for the control rat spleen sample (A), treated rat (2 weeks post-administration) spleen sample (B), control rat spleen spiked with TeO_3^{2-} (C), and control rat spleen spiked with QD705 (D). Each sample was respectively treated with 10 M HCl and PBS solutions before the chemical vaporization of ether the released or total Te species. The spike concentration was 0.1 μg Te L^{-1}.

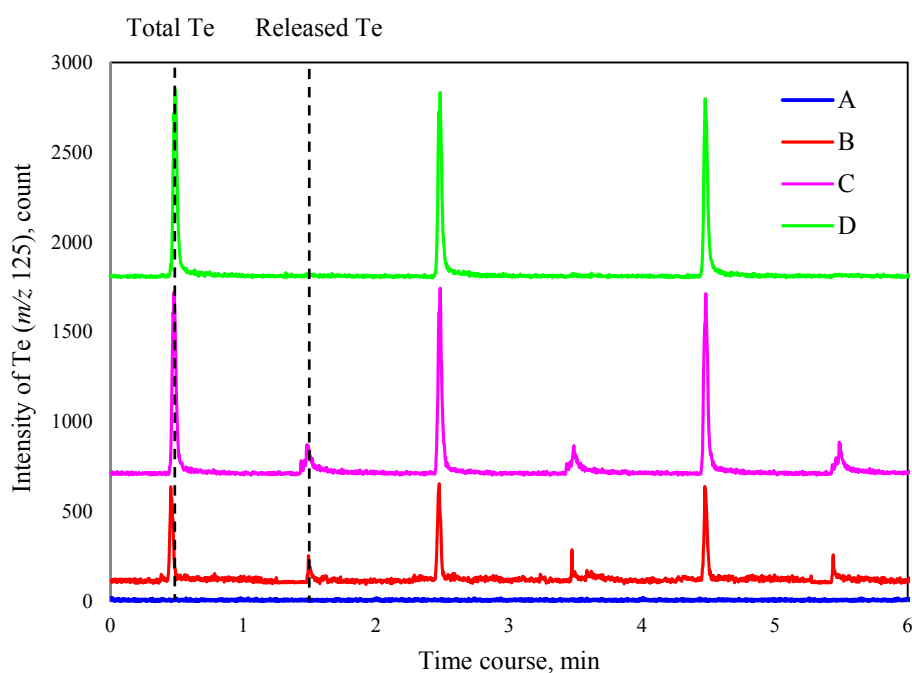**Table 1.** Operation sequence of the established HG-ICP-MS differentiation system

Step	Valve/Position	Time point	Function
1	A/Inject	0:55	Deliver the sample mixed with 10 M HCl for vaporization of total Te
2	A/Load	1:00	Load the sample mixed with 10 M HCl into sample loop
3	B/Inject	1:55	Deliver the sample mixed with PBS for vaporization of released Te
4	B/Load	2:00	Load the sample mixed with PBS into sample loop

Table 2. Optimized parameters for the developed HG-ICP-MS differentiation method

Chemical VG-based differentiation scheme	
Sample volume	10 μL
Conditioning solution for Te ions	10 mM PBS, pH 7.4
Conditioning solution for total Te	10M HCl
Reductant	0.05% $NaBH_4$ with 0.1% NaOH
Carrier solution	0.25 M HCl
Reductant flow rate	0.75 mL min^{-1}
Carrier solution flow rate	0.75 mL min^{-1}
Waste flow rate in GLS	2 mL min^{-1}
Sample loading time	5 s
Sample throughput	60 h^{-1}
ICP-MS	
ICP mass spectrometer	Agilent 7500a
Ar gas flow rates	
Plasma	15 L min^{-1}
Auxiliary	0.9 L min^{-1}
Nebulizer	1.28 L min^{-1}
Plasma forward power	1500 W
Sampling cone	Ni, 1-mm orifice
Skimmer cone	Ni, 0.4-mm orifice
Analysis mode	Time-resolved analysis
Integration time	50 ms
Isotope monitored	^{125}Te

Table 3. Analytical performance of the developed HG–ICP-MS method and routine ICP-MS analysis method for Te (*m/z* 125)

	working range, ng L^{-1}	*R*	MDL, ng L^{-1}
Ionic Te	10–500	0.9994	1.8
Total Te	10–500	0.9988	0.4
Total Te[*]	10–500	0.9993	8.8

*Experiments conducted with routine ICP-MS analysis to determine total Te concentrations in digested rat samples.

Table 4. Spike recoveries of TeO_3^{2-} and QD705 in rat organ/tissue samples

	Dissolved TeO_3^{2-}, %	Total TeO_3^{2-}, %	Total QD705, %
Blood	100 ± 3	103 ± 4	96 ± 3
Liver	107 ± 3	101 ± 1	111 ± 3
Liver*	88 ± 4	94 ± 2	91 ± 2
Spleen	118 ± 1	117 ± 1	103 ± 4
Kidney	92 ± 1	94 ± 3	85 ± 6
Lung	104 ± 2	95 ± 2	84 ± 1
Brain	105 ± 2	108 ± 2	117 ± 2

*Sample spiked with TeO_3^{2-} and QD705 respectively before Solvable^{TM} treatment.

Table 5. Quantitative Te-based QD705 biodistribution and dissolution 2 and 16 weeks

post-administration in (200 pmole kg^{-1} body weight; $n = 4$)

	2 weeks post-administration			16 weeks post-administration			
	Te conc.[a], µg kg^{-1}	Cd conc.[b], µg kg^{-1}	Te_r/Te_{total} ratio[a], %	Te conc.[a], µg kg^{-1}	Cd conc.[b], µg kg^{-1}	Te_r/Te_{total} ratio[a], %	p value[c]
Blood	4.8 ± 1.2	5.3 ± 0.5	17 ± 5	1.2 ± 0.3	0.9 ± 0.2	96 ± 14	0.0001
Liver	8.3 ± 1.2	1963.6 ± 187.9	55 ± 14	2.1 ± 0.3	282.4 ± 44.6	79 ± 8	0.0331
Spleen	10.3 ± 1.9	5048.3 ± 836.6	38 ± 5	2.0 ± 0.1	349.2 ± 81.9	74 ± 13	0.0009
Kidney	6.9 ± 1.9	1399.1 ± 554.2	73 ± 10	2.0 ± 0.4	709.3 ± 120.1	42 ± 19	0.0336
Lung	3.8 ± 0.9	226.7 ± 25.5	29 ± 6	1.4 ± 0.3	58.1 ± 9.5	26 ± 4	0.6665
Brain	1.1 ± 0.9	2.1 ± 0.5	35 ± 16	0.7 ± 0.4	1.4 ± 0.5	46 ± 17	0.4834

[a] The values were determined by our developed HG–ICP-MS scheme.

[b] The values were determined by routine ICP-MS analysis method.

[c] Statistical comparisons of Te_r/Te_{total} ratios between the two groups.